Chapter 5

Experiments

In this Chapter we present the experimental validation of the controllers designed in Chapter 4 and the policy management described in Chapter 1. The results are presented for each controller, *i.e.* for the full-bridge rectifier and the doubly-fed induction machine, separately. Finally, in the last section of this chapter the whole flywheel energy storage system power flow management is experimentally tested.

Part of the results of this Chapter can also be found in [8][13] [14].

5.1 Ac-dc boost rectifier

5.1.1 Experimental setup

The experimental setup is shown in Figures 5.1 and 5.2 and has the following parts:

- A full-bridge boost converter (depicted in Figure 5.2) with IGBT switches (Siemens BSM 25GD 100D) and parameters $r = 0.1\Omega$, $L = 1$mH and $C = 4500\mu$F. The switching frequency of the converter is 20 KHz and a synchronous centered-pulse single-update pulse-width modulation strategy is used to map the controller's output to the IGBT gate signals.

- The analog circuitry for the sensors. The AC main source, PMW and DC bus voltages and currents are sensed with isolation amplifiers. All the signals from the sensors pass through the corresponding gain conditioning stages to adapt their values to A/D converters.

- Control hardware and DSP implementation. The control algorithm is implemented using the Analog Devices DSP-21116 and DSP-21992 processors. The processing core of this device runs at 100MHz and has a 32bit floating-point unit. The sampling rate of the A/D channels has been selected at 20KHz, the same as the switching frequency of the full-bridge system.

- The nominal RMS AC mains voltage is $V_s = 48.9$V RMS and its nominal frequency is 50 Hz.

In order to achieve a bidirectional power flow in this isolated setup, a current source has been connected to the dc side of the converter.

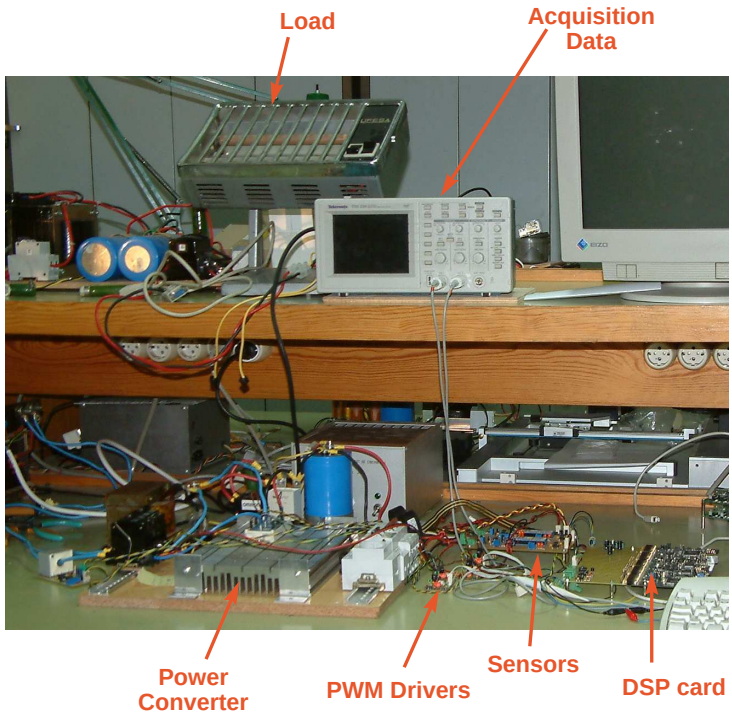

Figure 5.1: Experimental setup: full-bridge rectifier, DSP card, sensors, data acquisition.

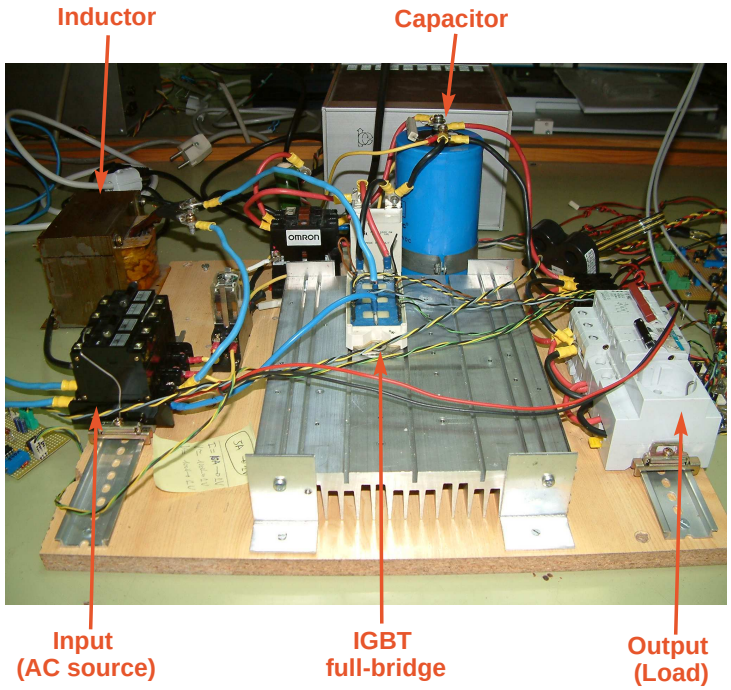

Figure 5.2: Experimental setup: full-bridge rectifier, DSP card, sensors, data acquisition.

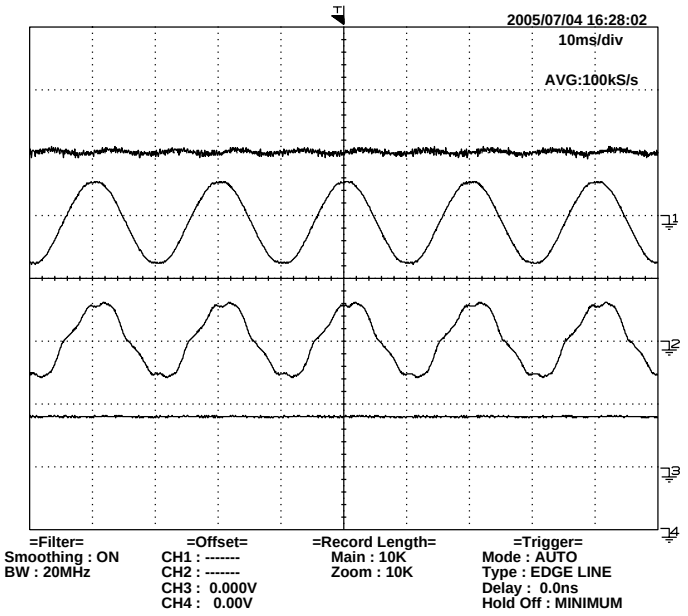

Figure 5.3: Experimental results: V, i and v_i for $i_l > 0$.

5.1.2 Experimental results

Experiment results are shown in Figures 5.3 - 5.9. First a test with a resistive load R_l connected was performed. Figures 5.3, 5.4 and 5.5 show the waveform of the grid current i and voltage v_i, the dc bus voltage V and the load current i_l. Figure 5.3 shows that the dc-bus voltage remains close to the desired value with an acceptable small oscillation. The grid voltage and current are nearly in phase (as shown by the power factor in Figure 5.5) but the waveform of the current displays a noticeable distortion with respect to the desired sinusoidal form, and some high order components of i do appear (Figure 5.4). This can be attributed to the sampling time and the dead-time of the IGBTs, which introduce 3rd and 5th harmonic components. The main problem using the GSSA approach is that the controller is transparent to these disregarded harmonics.

Figures 5.7, 5.8 and 5.9 display the results for $i_l < 0$. The experimental results are similar to the $i_l > 0$ case, but the inductor current i has a triangular shape. This problem can be traced to the fact that the 3rd current harmonic is not *controlled* and has the same sign than in the $i_l > 0$ case. For $i_l > 0$ the third harmonic is added to the first harmonic component, while in the $i_l < 0$ case, due to the current sign inversion, the third harmonic is subtracted.

These results validate both the IDA-PBC method and the GSSA decomposition of variables, *i.e.* the control goals of the considered harmonics are achieved. Further improvements of the controller, namely consideration of higher harmonics of the dc voltage and inductor current, are also under study, in order to improve the tracking of the ac voltage waveform.

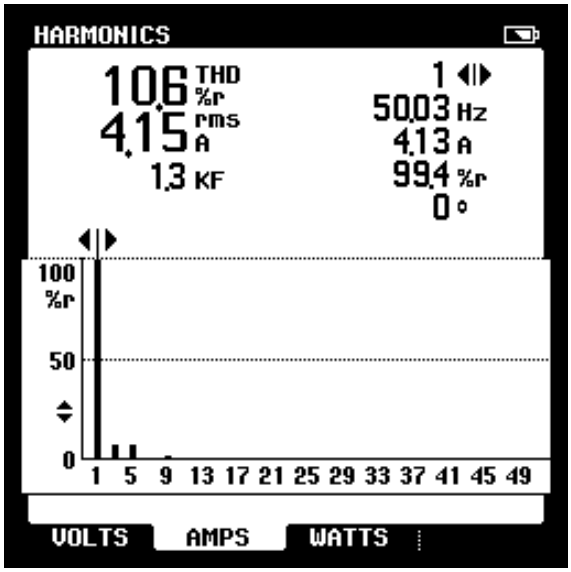

Figure 5.4: Experimental results: THD of the AC current i for $i_l > 0$.

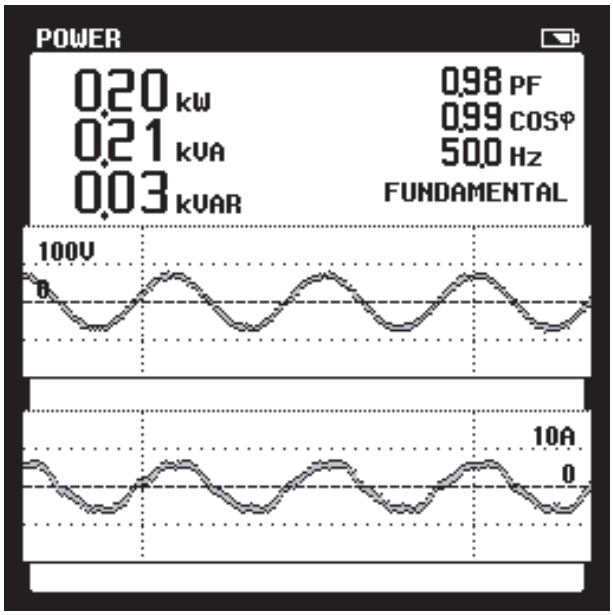

Figure 5.5: Experimental results: power factor for $i_l > 0$.

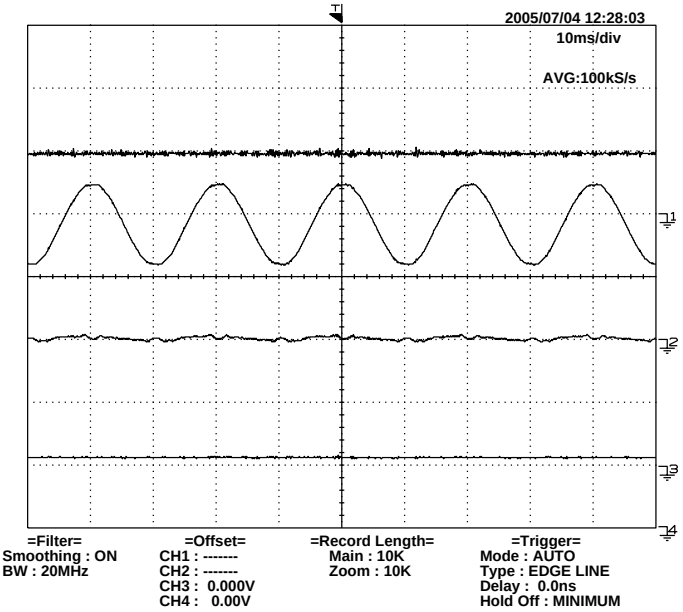

Figure 5.6: Experimental results: V, i and v_i for $i_l = 0$.

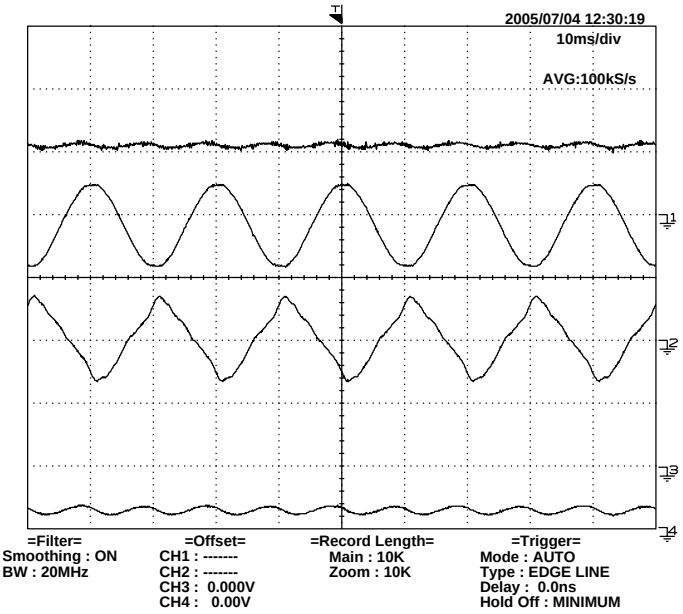

Figure 5.7: Experimental results: V, i and v_i for $i_l < 0$.

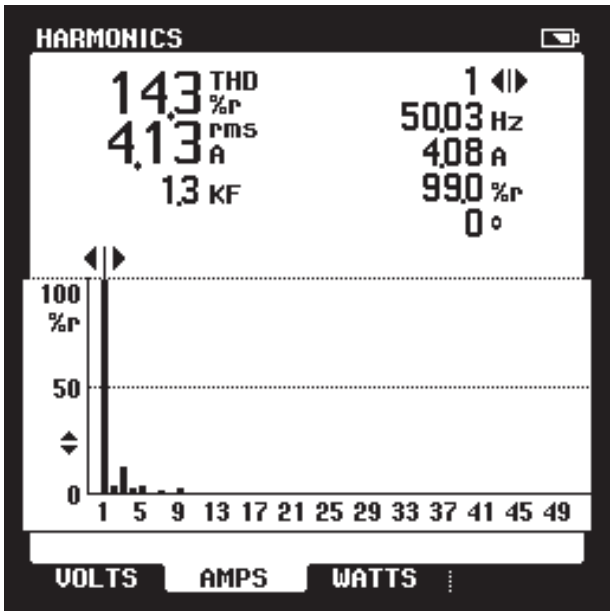

Figure 5.8: Experimental results: THD of the AC current $i$for $i_l < 0$.

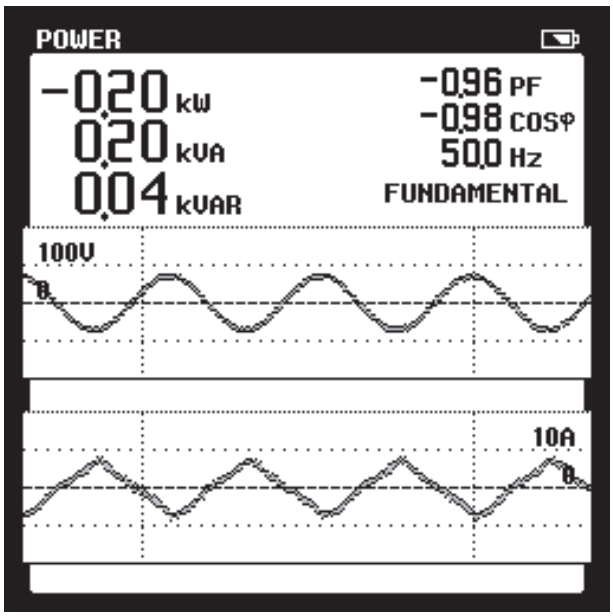

Figure 5.9: Experimental results: power factor for $i_l < 0$.

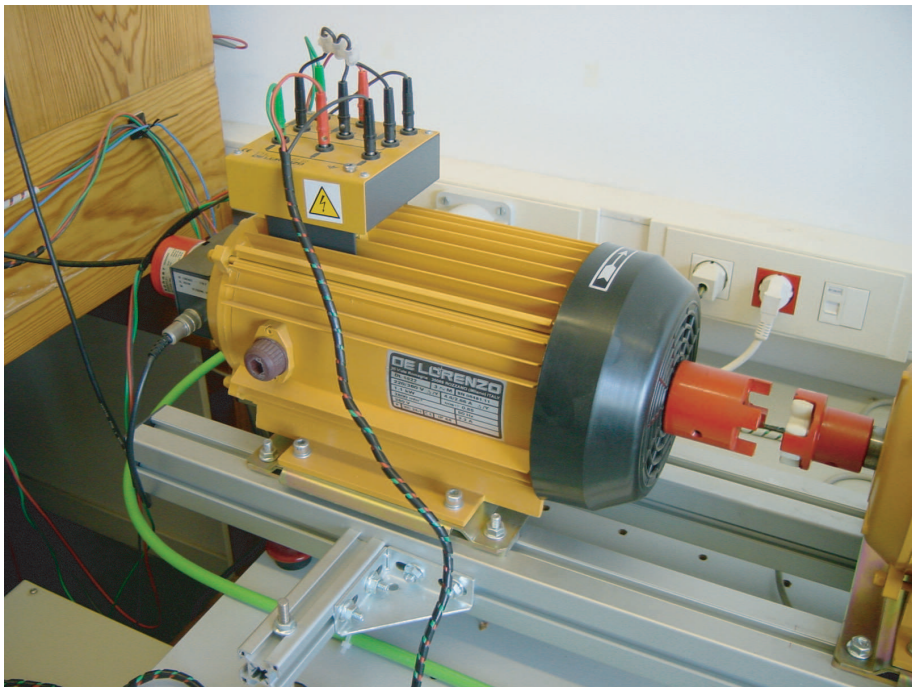

Figure 5.10: Experimental setup: a doubly-fed induction machine.

5.2 Doubly-fed induction machine

5.2.1 Experimental setup

For the experimental setup we used a 1.1kW, voltage fed 220/380V (Δ/Y), nominal current 4.8/2.4A (Δ/Y), 50Hz 2-pole machine (DeLorenzo DL 1022K), see Figure 5.10. The machine parameters are: $R_s = 4.92\Omega$, $R_r = 4.42\Omega$, $L_s = 7.25$mH, $L_r = 7.15$mH, $L_{sr} = 7.1$mH, star shape stator and rotor connection, $J_m = 0.00512\text{Kg}\cdot\text{m}^2$, $B_r = 0.005\text{N}\cdot\text{m}\cdot\text{rad}^{-1}\text{s}^{-1}$.

The control algorithm is coded into a computer running with RTLinux (Real Time Linux), using RTiC-Lab (Real Time Controls Laboratory), which allows to change control parameters in real time. The sampling rate has been selected at 10KHz. The RTLinux interfaces the IGBTs of the 3-phase inverter and generates the PWM signals appropriate to implement the DFIM controller. The appearance of the RTiC-Lab environment is displayed in Figure 5.11.

The control hardware consists of:

- PC computer: Pentium IV, 1.8 GHz, 512MB RAM.
- A/D card: 3 PCI-DAS 4020/12 modules. Ultra High-speed PCI- bus compatible, 4-Channel, 12-Bit Analog Input Board with two Analog Output Channels and 24 Digital I/O Channels.
- PWM card: NuDAQ PCI-8133. 3-Channel quadrature encoder counters for a PCI PnP-bus an a 12-Bit PWM waveform generators.

Figure 5.12 shows the signal connection scheme between the system and the control

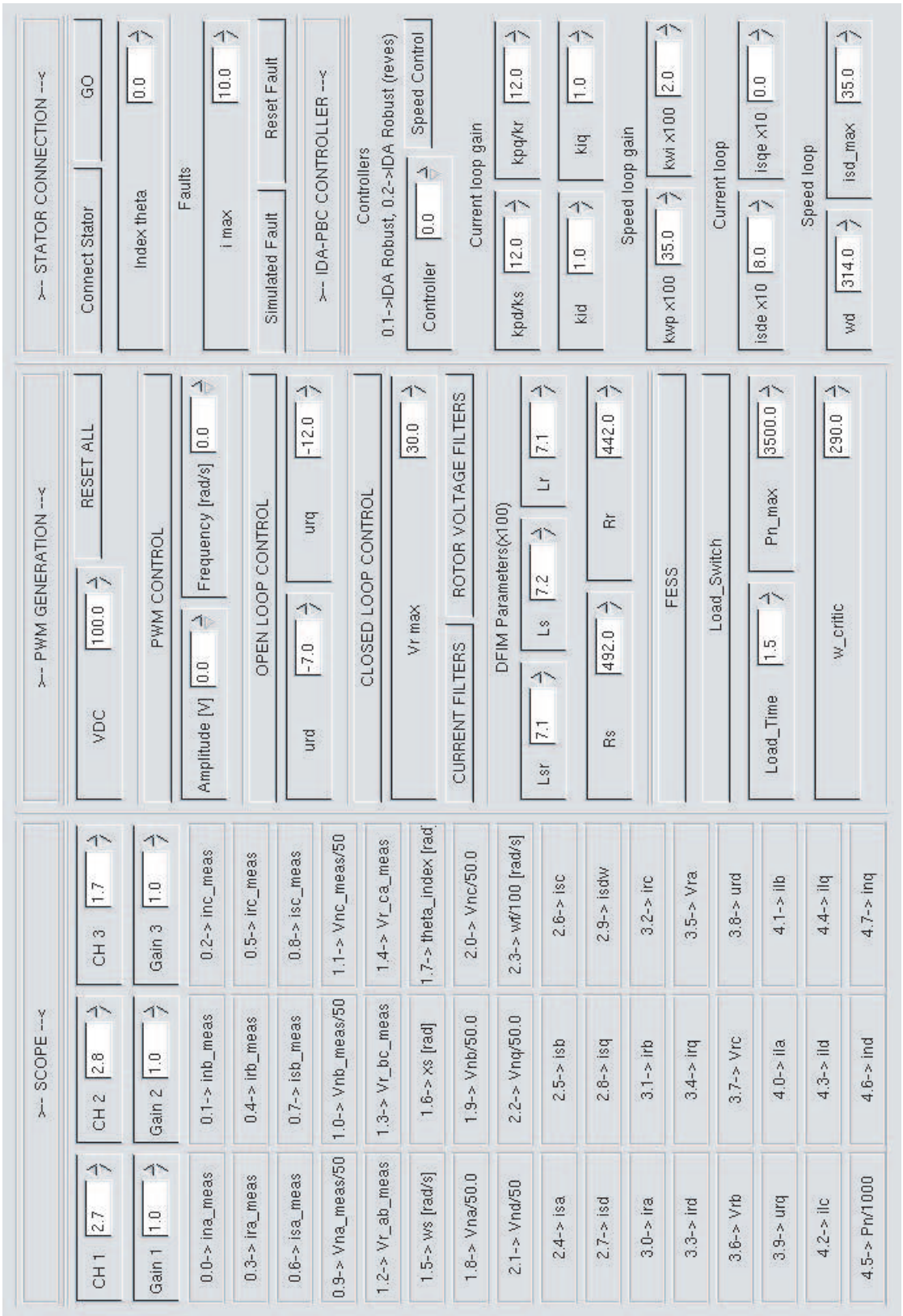

Figure 5.11: Experimental setup: RTiC screen appearance.

hardware.[1]

5.2.2 Experimental results

The experimental test consist in speeding up the machine from $\omega^* = 310\text{rad s}^{-1}$ to $\omega^* = 325\text{rad s}^{-1}$ and coming back to $\omega^* = 310\text{rad s}^{-1}$, while at the same time controlling the reactive power of the machine through i_{sq}. The control gains are set at $k = 12$, $k_i = 2$, $k_{\omega p} = 0.35$ and $k_{\omega i} = 0.01$. Experimental results are shown in Figures 5.22 to 5.17.

In Figure 5.22 the mechanical speed is depicted. Figure 5.14 shows the dq-stator current components. Notice that i_{sq} remains close to zero, which means that the power factor of the stator side is very small, see also Figure 5.15. Finally, in Figures 5.16 and 5.17 the control action v_r and its corresponding a-phase are depicted.

5.3 Experiments of the flywheel energy storage system

In this section we present the experimental setup and the experimental results of the Flywheel Energy Storage System.

5.3.1 Experimental setup

The experimental setup consists of the DFIM described extensively in Section 5.2 controlled through a back-to-back converter. Figure 5.19 shows the full-bridge rectifier described in Section 5.1, coupled to a 3-phase DC/AC inverter containing

- a power module pack of six IGBT switches Siemens BSM 15 GD 120 D2 (1200V, 25A).

The PWM signal is generated with the hardware described in Section 5.2.

Figure 5.20 shows the DFIM coupled to a flywheel and the local load. In order to increase the range of available parameters in the experimental setup the flywheel is split into two separate ones, and the local load is made up of three variable resistors.

- The flywheels have a moment of inertia $J_f = 0.055\text{Kg m}^2$ each one, which gives a total inertia $J_m = 0.11512\text{Kg m}^2$ (tacking into account the DFIM inertia).
- The three local load resistors have $R = 37/68/89\Omega$, respectively.

5.3.2 Experimental results

Experimental results are shown in Figures 5.21 to 5.25. The maximal power network delivered by the load is fixed at $P_n = 3300\text{W}$. The DFIM starts at the optimal speed ($\omega = 314\text{rad s}^{-1}$). A resistive load, which requires $P_l = 4180\text{W}$, is connected for 1 second. The control parameters are set to $k = 12$, $k_i = 2$, $k_{\omega p} = 0.35$ and $k_{\omega i} = 0.01$.

Figure 5.21 shows that the power delivered by the load remains close to the desired value even if the connected load requires more power. This is due to the fact that the mechanical speed of the DFIM (and the flywheel) decreases, see Figure 5.22, providing thus the required extra energy, and when the load is disconnected the mechanical speed returns to the optimal value.

[1] The hardware of another plant [22], called Joint System (JS), which shares some elements with ours (FW), is also displayed.

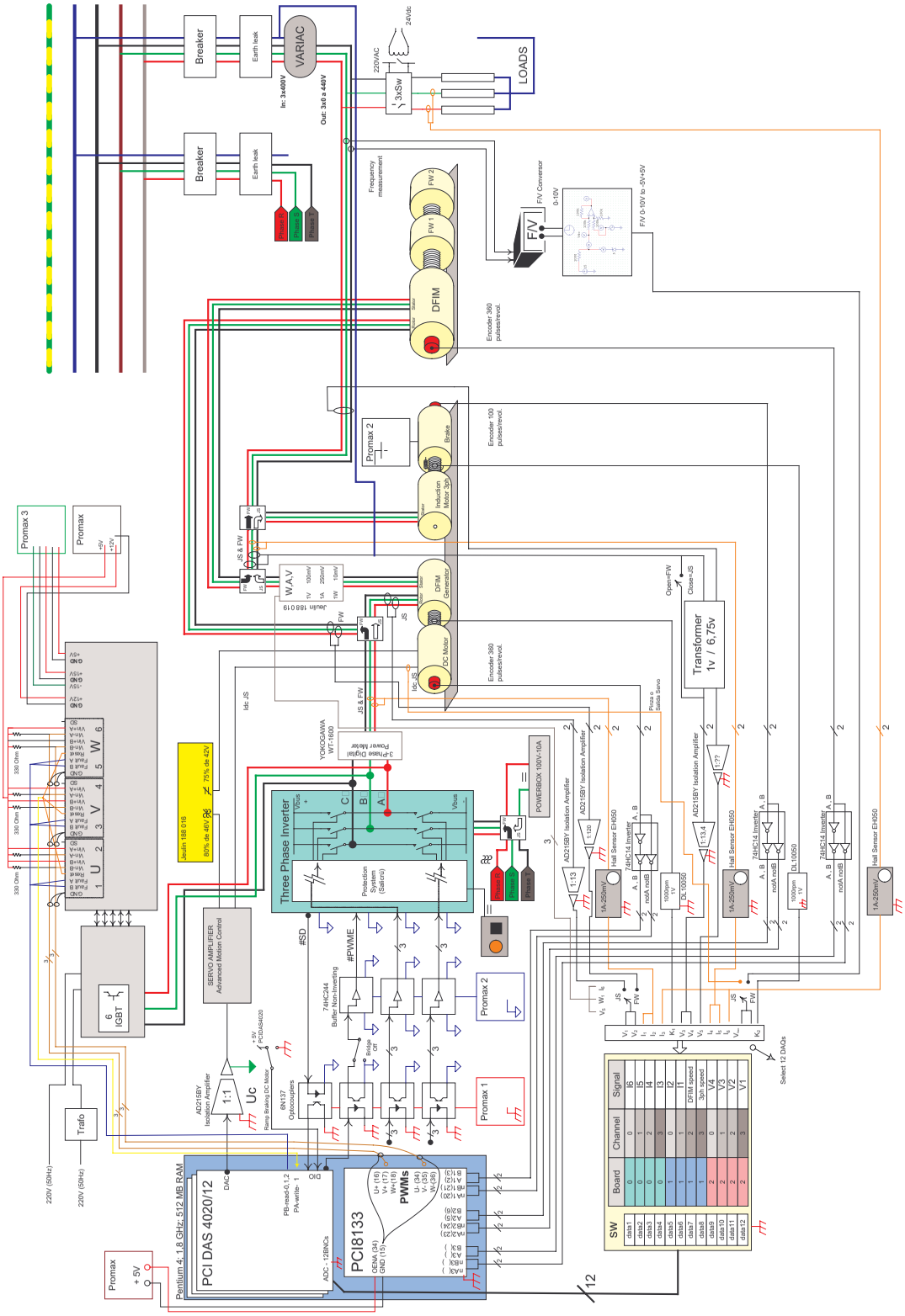

Figure 5.12: Experimental setup: Interconnection scheme.

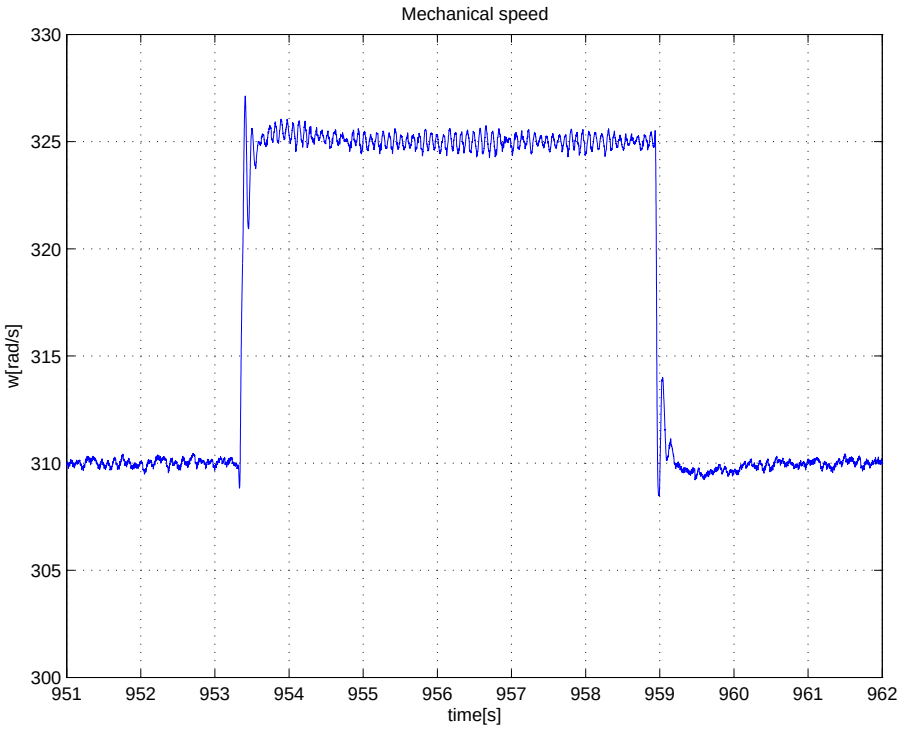

Figure 5.13: Experimental results: mechanical speed ω.

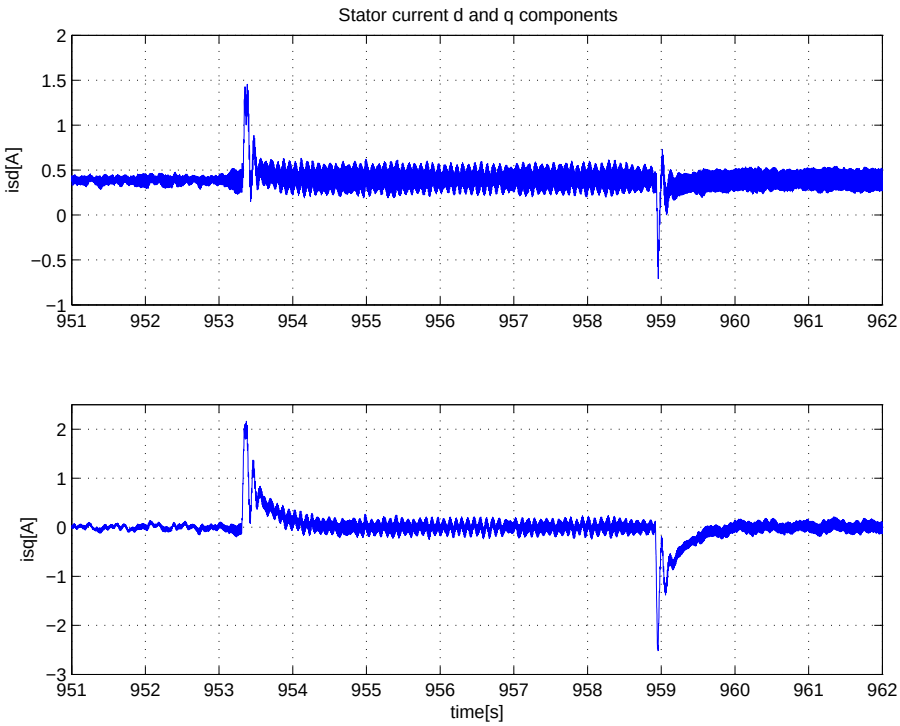

Figure 5.14: Experimental results: stator current d and q components.

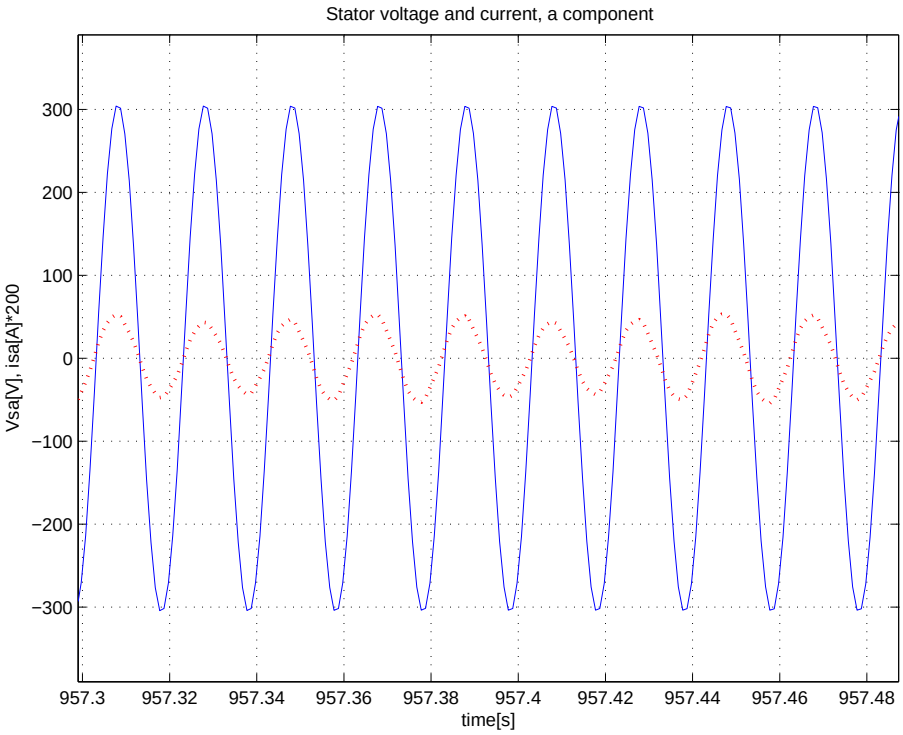

Figure 5.15: Experimental results: a-stator voltage and current, v_{sa} and i_{sa}.

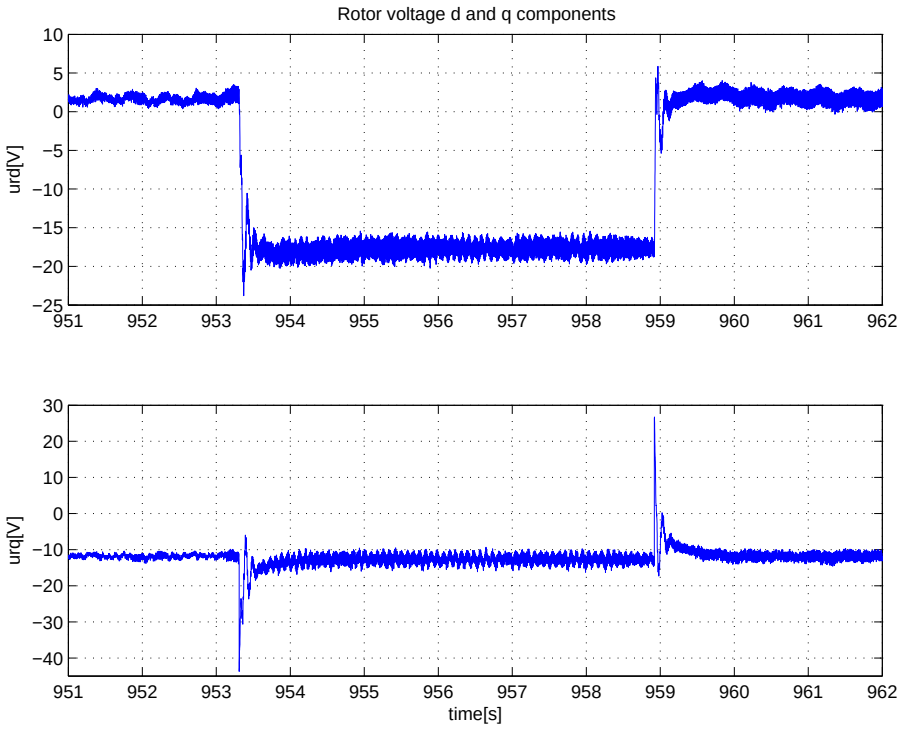

Figure 5.16: Experimental results: rotor voltage d and q components.

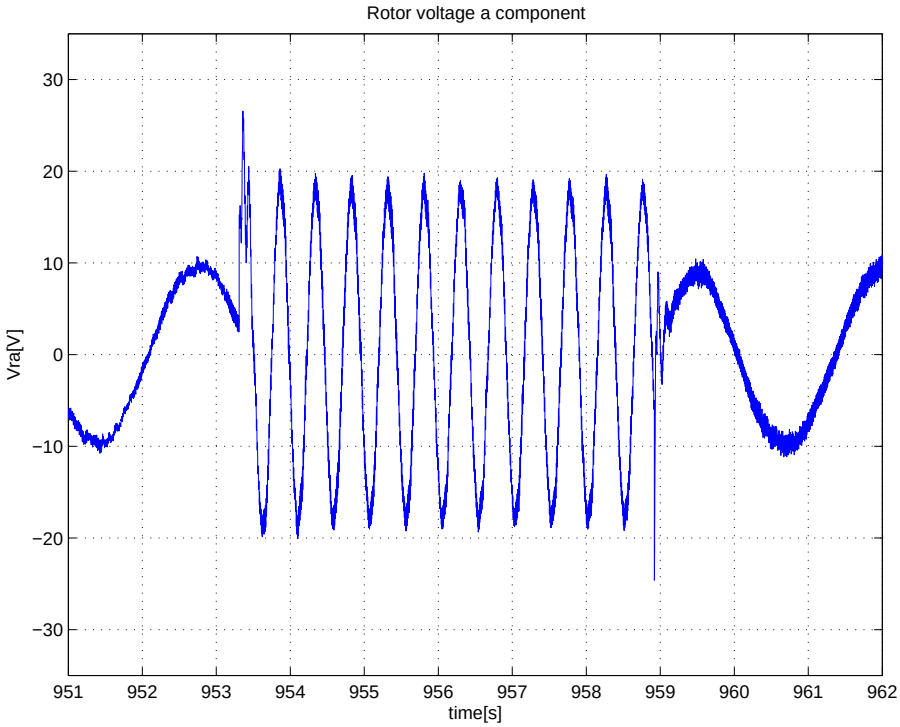

Figure 5.17: Experimental results: rotor voltage a component.

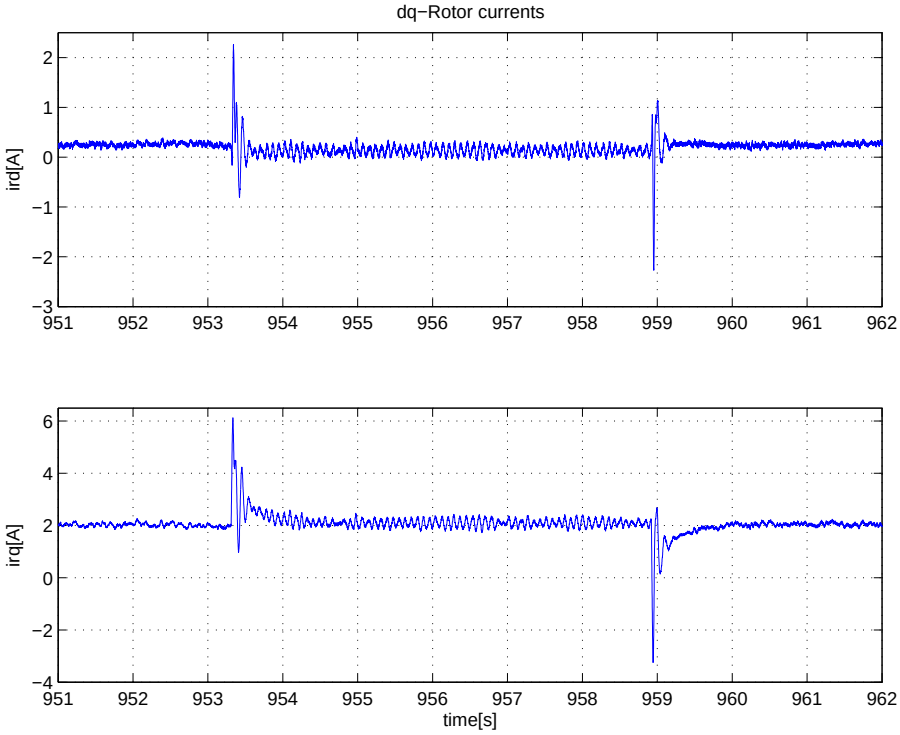

Figure 5.18: Experimental results: rotor current d and q components.

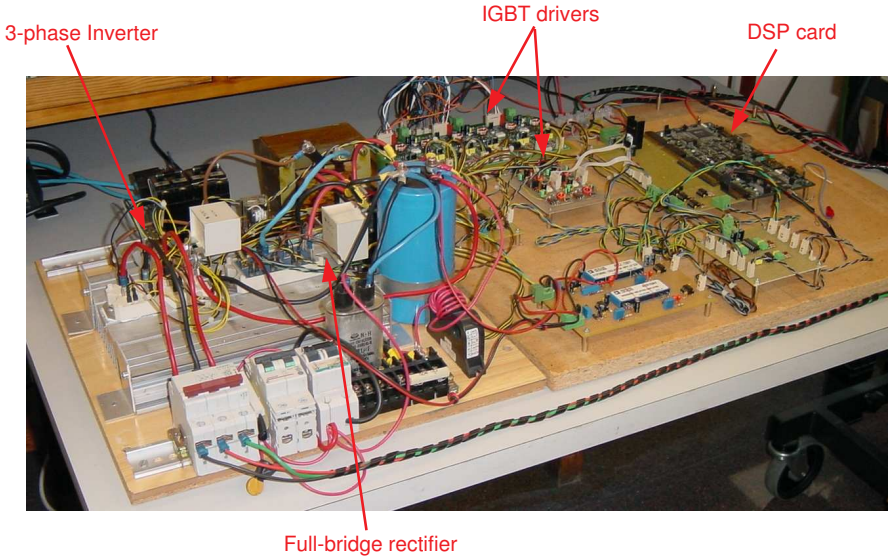

Figure 5.19: Experimental setup: The B2B converter.

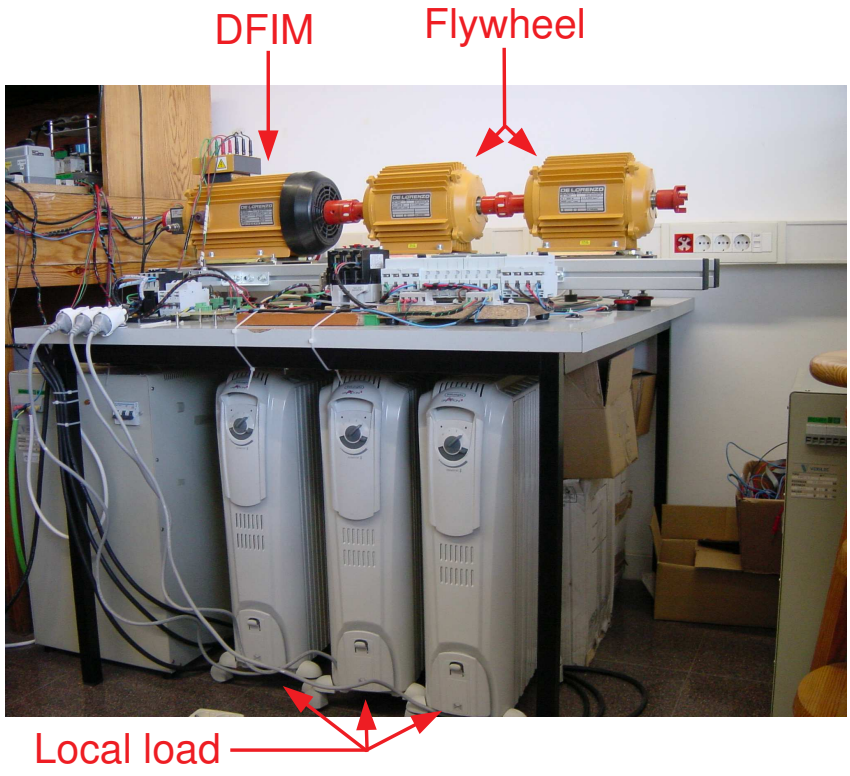

Figure 5.20: Experimental setup: The DFIM coupled to a flywheel and the local load.

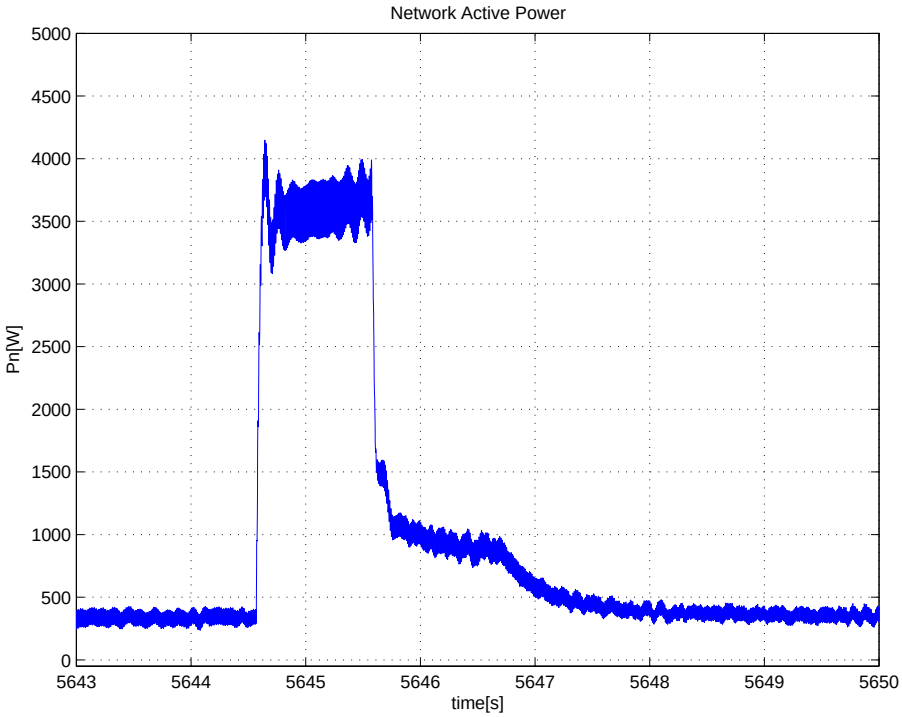

Figure 5.21: Experimental results: network active power, P_n.

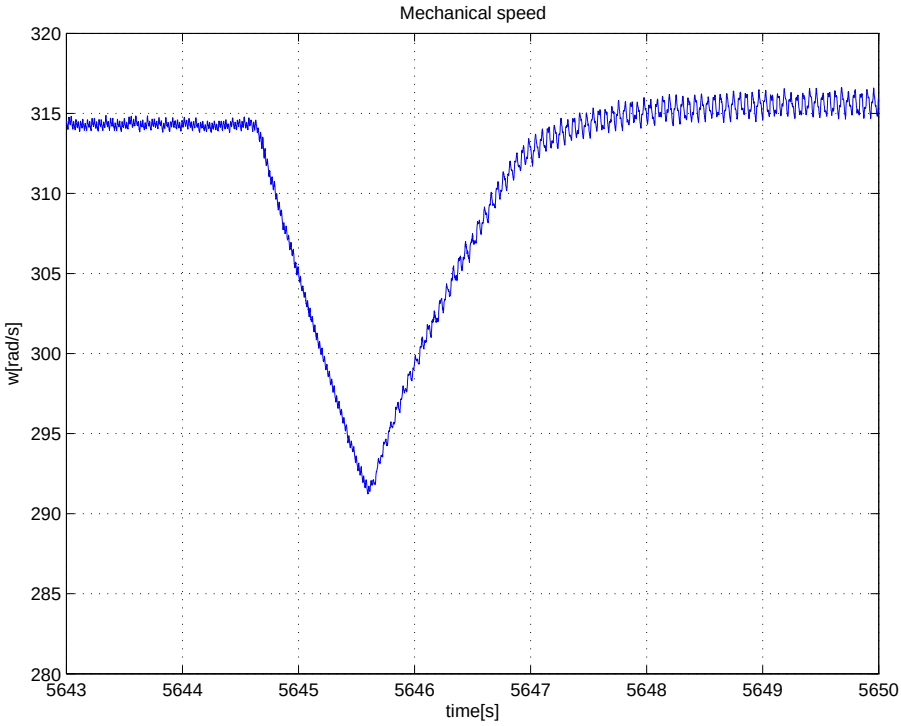

Figure 5.22: Experimental results: mechanical speed, ω.

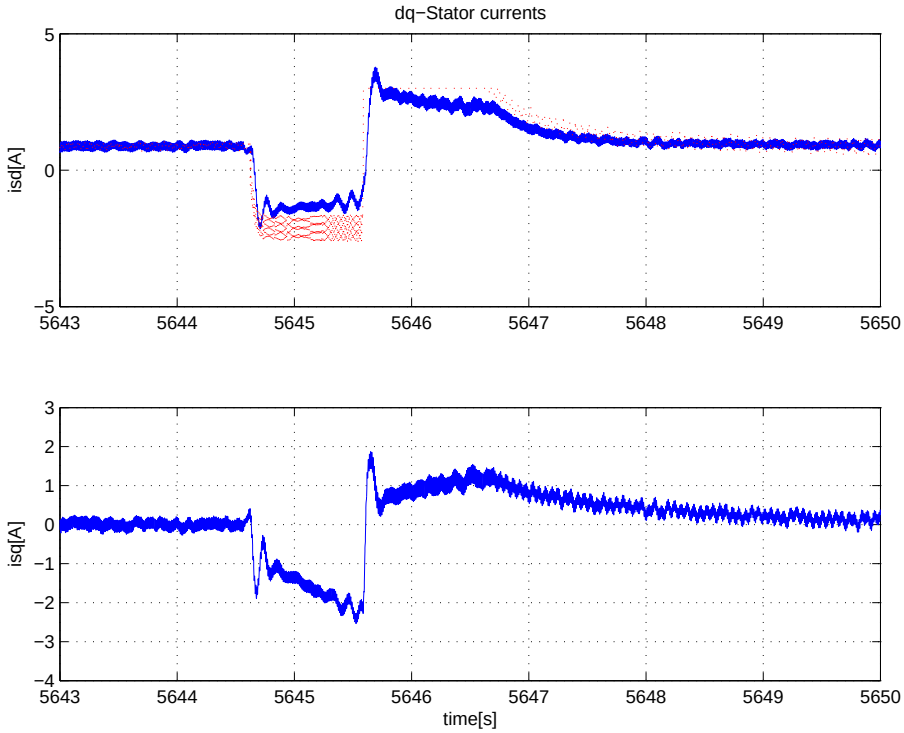

Figure 5.23: Experimental results: stator dq-currents, i_{sd} and i_{sq}.

The dq stator currents are depicted in Figure 5.23. Since the stator voltage reference is used to transform the original variables, i_{sd} represents the active power flowing through the stator side of the DFIM and i_{sq} the reactive power. It can be seen that the reactive power supplied by the grid tends to zero (the local load is purely resistive and the DFIM only consumes active power).

Finally, Figures 5.24 and 5.25 show the control action u_r and the corresponding a-phase of the rotor voltages, V_{ra}.

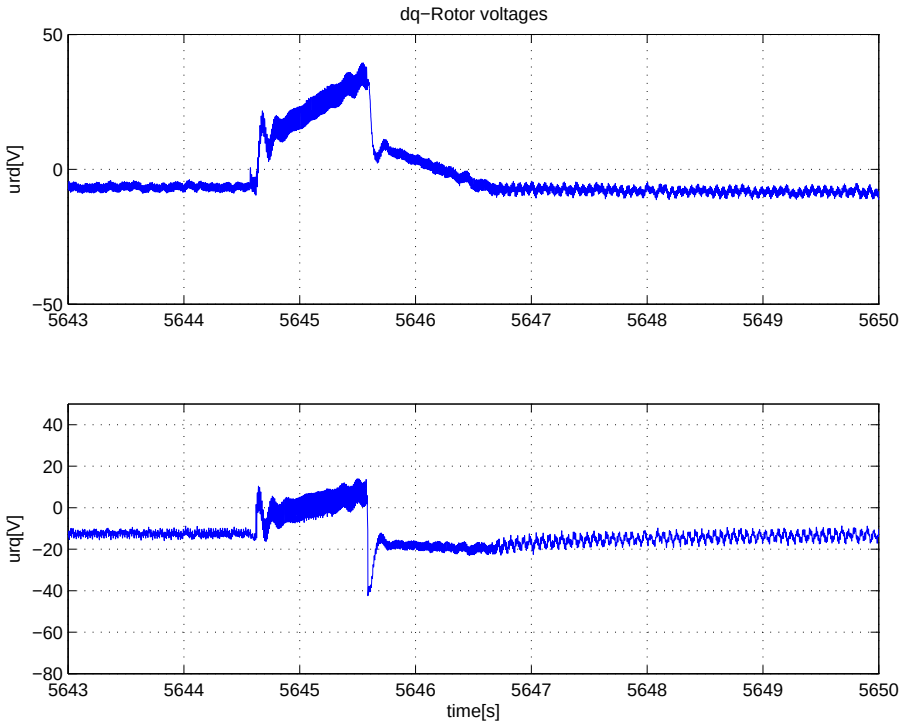

Figure 5.24: Experimental results: rotor dq-voltages, u_{rd} and u_{rq}.

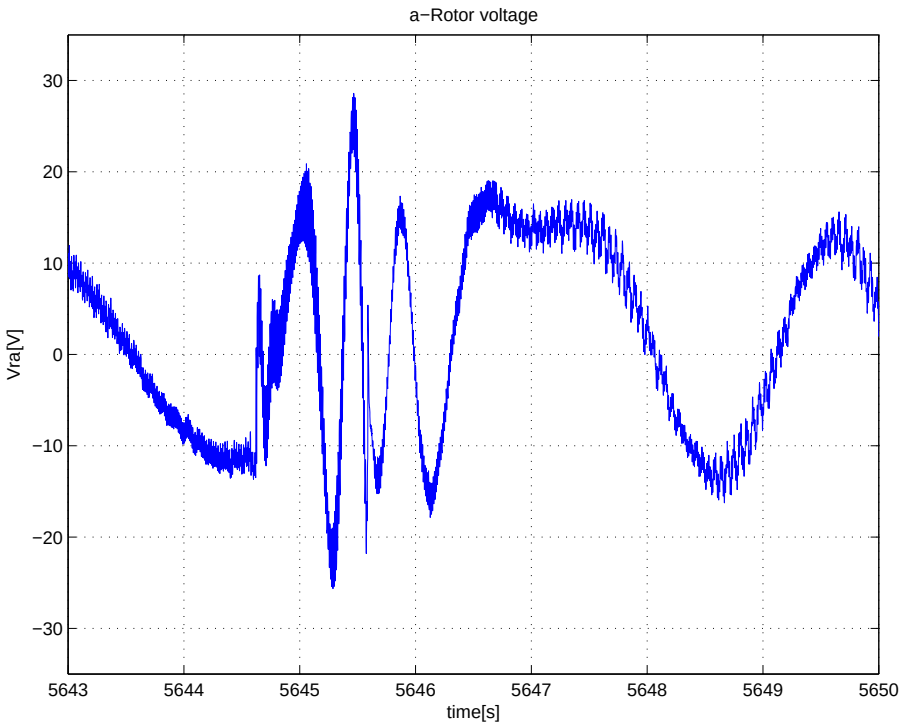

Figure 5.25: Experimental results: rotor a-voltage, V_{ra}.